

## Observations of Counter-Current Toroidal Rotation in Alcator C-Mod LHCD Plasmas

J.E. Rice 1), A.C. Ince-Cushman 1), P.T. Bonoli 1), M.J. Greenwald 1), J.W. Hughes 1), R.R. Parker 1), M.L. Reinke 1), G.M. Wallace 1), C.L. Fiore 1), R.S. Granetz 1), A.E. Hubbard 1), J.H. Irby 1), E.S. Marmor 1), S. Shiraiwa 1), S.M. Wolfe 1), S.J. Wukitch 1), M. Bitter 2), K. Hill 2) and J.R. Wilson 2)

1) Plasma Science and Fusion Center, MIT, Cambridge, MA, USA

2) Princeton Plasma Physics Laboratory, Princeton, NJ, USA

e-mail contact of main author: rice@psfc.mit.edu

**Abstract.** Following application of lower hybrid current drive (LHCD) power, the core toroidal rotation in Alcator C-Mod L- and H-mode plasmas is found to increment in the counter-current direction, in conjunction with a decrease in the plasma internal inductance,  $l_i$ . Along with the drops in  $l_i$  and the core rotation velocity, there is peaking of the electron and impurity density profiles, as well as the ion and electron temperature profiles. The mechanism generating the counter-current rotation is unknown, but it is consistent with an inward shift of energetic electron orbits, giving rise to a negative core radial electric field. The peaking in the density, toroidal rotation (in the counter-current direction) and temperature profiles occurs over a time scale similar to the current relaxation time but slow compared to the energy and momentum confinement times. Most of these discharges exhibit sawtooth oscillations throughout, with the inversion radius shifting inward during the LHCD and profile evolution. The magnitudes of the changes in the internal inductance and the central rotation velocity are strongly correlated and found to increase with increasing LHCD power and decreasing electron density. The maximum effect is found with a waveguide phasing of  $60^\circ$  (a launched parallel index of refraction  $n_{\parallel}$  of 1.5), with a significantly smaller magnitude at  $120^\circ$  ( $n_{\parallel} \sim 3.1$ ), and with no effect for negative or heating ( $180^\circ$ ) phasing. These results mimic the current drive efficiency which scales as  $P_{LH}/n_e n_{\parallel}^2$ . Regardless of the plasma parameters and launched  $n_{\parallel}$  of the waves, there is a strong correlation between the rotation velocity and  $l_i$  changes, possibly providing a clue for the underlying mechanism.

### 1. Introduction

In order for tokamaks to be viable candidates for future steady state fusion reactors, some variety of non-inductive current drive is necessary. Lower hybrid current drive (LHCD) [1] has been successfully implemented in lower electron density plasmas [2-4], and an outstanding issue is the extension to higher densities and under conditions relevant for reactors [5]. Another approach for non-inductive current drive is to take advantage of the bootstrap current [6] generated by the large pressure (density and temperature) gradients in plasmas with internal transport barriers (ITBs) [7,8]. Challenges of this approach involve production of steady state ITBs (without current ramping) under reactor relevant conditions (without neutral beam injection) and control of the barrier foot location. H-mode plasmas with ITBs having pressure gradients in excess of 2.5 MPa/m have been obtained in Alcator C-Mod with ion cyclotron range of frequencies (ICRF) heating [9-14]. ITBs have also been formed without neutral beam injection in lower hybrid current drive (LHCD) and electron cyclotron current drive (ECCD) plasmas in other devices [15-17]. Another issue for future tokamak reactors is the generation and control of rotation velocity profiles for resistive wall mode (RWM) suppression [18,19] in the absence of external momentum input [20].

The three areas of LHCD [5], ITB formation [14] without current ramping or external momentum input and self-generated flows [21] are important components of the Alcator C-Mod research program, and will all be addressed here. C-Mod [22] is a compact ( $R \sim 0.67$  m,  $r \sim 0.21$  m), high field ( $B_T < 8$  T) device which can operate with electron densities in the range

from  $10^{19}$ - $10^{21}/\text{m}^3$ . Auxiliary heating is provided with up to 6MW of ICRF power. Dimensionless plasma parameters in the following ranges have been achieved:  $0.2 < \beta_N < 1.8$ ,  $0.01 < v^* < 20$  and  $170 < 1/\rho^* < 500$ . Non-inductive current is driven with LH waves injected from an 88 waveguide launcher capable of delivering up to 1.2 MW of power at 4.6 GHz with a parallel index of refraction,  $n_{\parallel}$ , in the range of 1.5-4 (waveguide phasing between  $60^\circ$  and  $150^\circ$ ), in both the co- and counter-current direction [5]. Time resolved toroidal rotation velocity and ion temperature profiles have been measured with an imaging Johann x-ray spectrometer system, from the Doppler shifts and broadening of argon and molybdenum x-ray emission lines [23]. Electron density profile evolution was determined using a laser interferometer and Thomson scattering system, electron temperature profiles were measured using Thomson scattering and a variety of ECE diagnostics and x-ray emission profiles were recorded with a diode array [24]. Unfortunately, the motional Stark effect diagnostic was not available for current density profile measurements in the discharges presented here; information on the current density comes from the internal inductance  $l_i$ , a measure of the peakedness of the current density profile, observations of sawtooth patterns and EFIT [25] magnetics reconstructions.

An outline of the paper is as follows: LHCD discharge time histories and parameter profiles will be presented in 2, followed by scaling studies in 3, with a discussion and conclusions in 4.

## 2. Observed Rotation Time Histories and Profile Evolution

In order to optimize performance in advanced tokamak operation, LHCD has been applied to a variety of different plasma types under a wide parameter range: lower, double and upper null L-mode target discharges with  $B_T$  in the range from 3.8 to 6.2 T, currents from 0.6 to 1.0

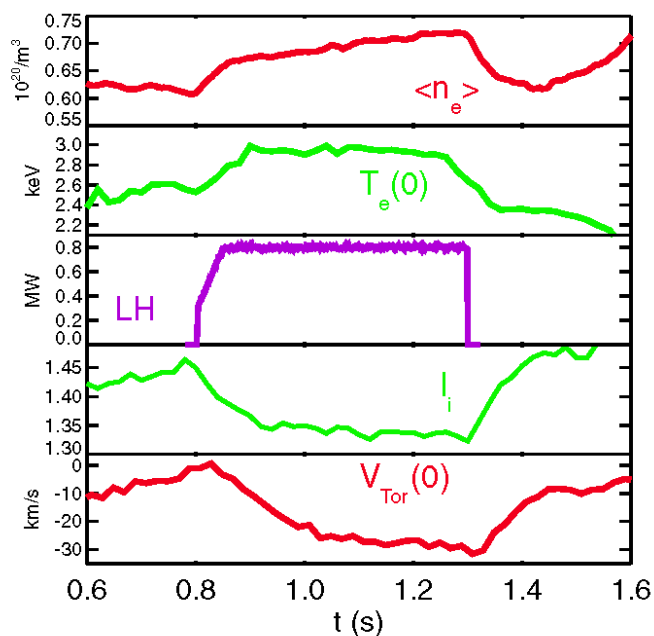


FIG.1. The electron density, electron temperature, LHCD power, internal inductance and central toroidal rotation for a 5.4 T, 0.8 MA L-mode discharge.

MA and electron densities from  $0.4$  to  $1.2 \times 10^{20}/\text{m}^3$ , in addition to H-mode target plasmas. LHCD power levels between 0.4 and 1.1 MW have been injected with  $n_{\parallel}$  in the range of 1.5-4, both co- and counter-current, including pure heating phasing. Shown in Fig.1 are the time histories of several parameters of interest for a low density 5.4 T, 0.8 MA L-mode discharge with LHCD. Following application of 0.8 MW of power between 0.8 and 1.3 s (with a launched  $n_{\parallel} \sim 2.3$ ), there was an increase in the core electron density and temperature, a drop in the internal inductance (consistent with a broadening of the current density profile) and an increment of the central toroidal rotation velocity in the counter-current

direction [26]. (Here a negative velocity corresponds to counter-current rotation.) Modeling indicates that about 250 kA were driven by LH waves in this case. The time scale for all of

these changes is of order of 100s of ms, similar to the current relaxation time ( $\tau_{CR}=1.4a^2kT_e^{1.5}/Z_{eff} \sim 250$  ms), but much longer than the energy [27] or momentum [28,29] confinement times ( $\sim 35$  ms). The time evolutions of the internal inductance and the toroidal rotation velocity are similar, suggesting a connection between the two quantities.

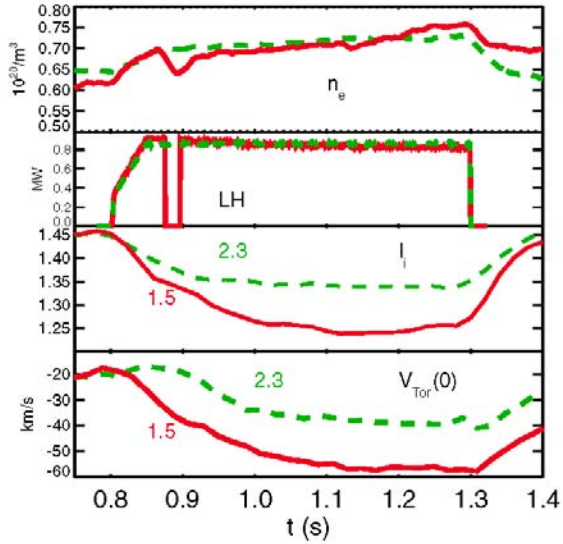


FIG.2. A comparison of two similar discharges with  $n_{||} \sim 1.55$  (red solid) and  $n_{||} \sim 2.3$  (green dashed).

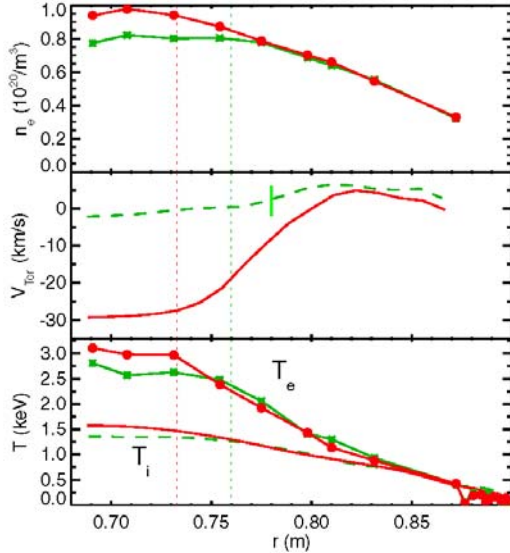


FIG.3. Electron density (top), toroidal rotation velocity (middle) and electron and ion temperature (bottom) profiles before (green dashed, asterisks) and during (solid red, dots) LHCD.

The magnitude of the changes in the internal inductance and core rotation velocity depend on the  $n_{||}$  spectrum of the launched waves [26]. Shown in Fig.2 is a comparison of two similar plasmas with different waveguide phasings. The discharge shown in red had an  $n_{||} \sim 1.55$  and demonstrated a much larger drop in  $l_i$  and  $V_{Tor}$  than the discharge shown in green dashed, with  $n_{||} \sim 2.3$ . This further emphasizes the connection between the rotation and internal inductance in LHCD plasmas.

The increases in density and temperature, and drops in rotation during LHCD occur in the very core of the plasma [26]. Shown in Fig.3 are the density, velocity and temperature profiles for the discharge of Fig.1 at two different times, before (0.75 s) and during (1.15 s) LHCD. There is a peaking of the electron density profile inside of  $R = 0.775$  m ( $r/a \sim 0.4$ ) during LHCD, while outside of this radius the profile remains unchanged. Similar behavior is seen in the electron and ion temperature profiles, with a peaking occurring inside of  $R = 0.755$  m during LHCD. Before LHCD, the velocity profile is rather flat and close to stagnant, while during LHCD, the profile is strongly centrally peaked in the counter-current direction. During LHCD, the sawtooth inversion radius moves inward to  $R \sim 0.73$  m from the target location of  $R \sim 0.76$  m. All of the profiles are relatively flat inside of the inversion radii both before and during LHCD. A flattening of the rotation velocity profile inside of the sawtooth inversion radius has been observed in TCV plasmas [30,31].

### 3. Scalings

Parameter scans of target plasma density, LHCD power and waveguide phasing have been undertaken in order to optimize performance. Shown in Fig.4 are results from a shot to shot power scan with a launched  $n_{||} \sim 2.3$  into 0.8 MA, 5.4 T target plasmas. In the top frame is the density peaking factor, the ratio of the central density to that at  $r/a = 0.7$ ; there is a steady increase in the density peaking with LHCD power. Similar behavior is seen in the ion temperature, as shown in the middle frame; the change in the central ion temperature (compared to the pre-LHCD level) also increases with injected power. In the bottom frame is the magnitude of the change in the central rotation velocity (always in the counter-current direction), comparing before and during LHCD, and there is a similar scaling with power. The vertical bands of points near the power level of 0.44 MW are due to variations in electron density. Shown in Fig.5 are the same three peaking parameters as a function of electron density for a series of 0.8 MA, 5.4 T discharges at fixed power (0.42 to 0.47 MW) with  $n_{||} \sim 2.3$ . For all three of these parameters, there is a decrease with increasing electron density. These trends with LHCD power and electron density suggest a similarity to the current drive efficiency, which scales the same way. Similar behavior in the density and temperature profile peaking also holds.

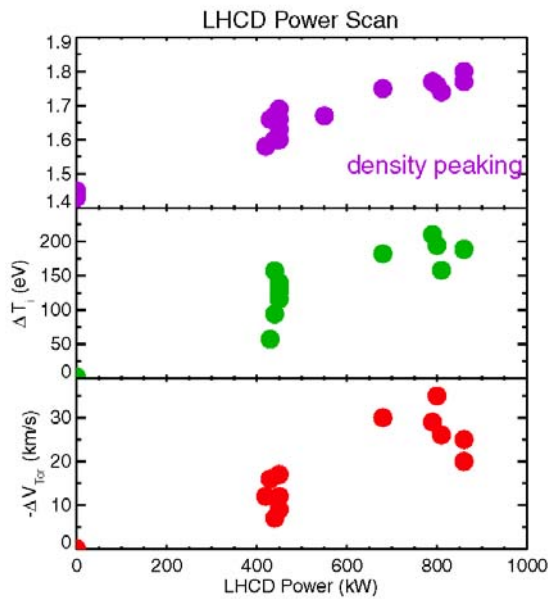


FIG.4. Density peaking factor (top), change in the central ion temperature (middle) and the change in the central rotation velocity (bottom) as a function of LHCD power.

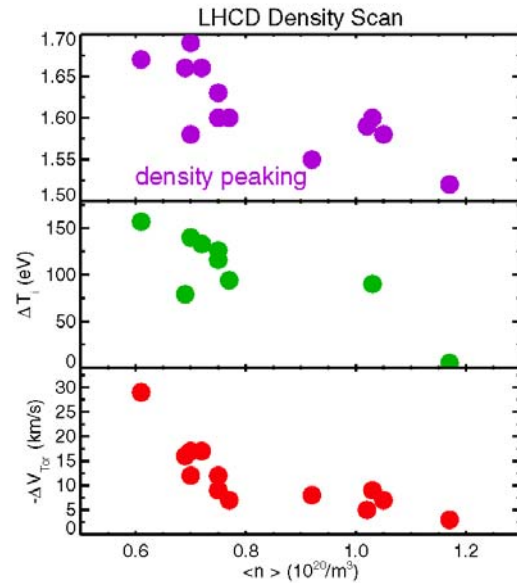


FIG.5. Peaking parameters (as in Fig.4) as a function of electron density at fixed LHCD power.

As is evident from Figs.1 and 2, the changes in internal inductance and rotation velocity are well correlated, regardless of plasma conditions or launched  $n_{||}$ . This point is emphasized in Fig.6 which shows the magnitude of the change in the rotation velocity as a function of the change in  $l_i$ , for a large number of discharges, regardless of plasma or LHCD parameters. The points in this figure represent a range of electron density from 0.4 to  $1.2 \times 10^{20}/\text{m}^3$ , toroidal magnetic field from 3.8 to 6.2 T, plasma current from 0.6 to 1.0 MA and LHCD power from 0.4 to 1.1 MW, with a variety of magnetic configurations. The points are sorted by launched  $n_{||}$  between  $\sim 1.5$  and 3.1. For waves directed counter-current, with  $n_{||} \sim -1.5$  and  $-2.3$ , there is very little effect.

#### 4. Discussion and Conclusions

Counter-current rotation during LHCD implies that the radial electric field is negative in the core region [26]. A negative core  $E_r$  indicates that there is an inward shift of electron orbits (or an outward shift of ion orbits). The fast electrons generated by LHCD experience an increase in  $|v_{||}|$  and hence an increase in their curvature drift velocity, whose sign is such that their orbits contract [26]. These fast electrons slow down through collisions on flux surfaces radially inward of the ones on which they were born, which constitutes a radial current and results in a negative  $E_r$ . Another possible mechanism for the negative core  $E_r$  is a resonant trapped particle pinch [32], which results from the canonical angular momentum absorbed by the trapped electrons which interact with the LH waves. Since the resonant particles are relatively collisionless, the added momentum cannot be readily lost, and they are forced to drift radially inward. While these fast electron models may explain the direction of the observed rotation, whether they can account for the velocity profile evolution time scale remains an open question.

In summary, substantial counter-current rotation has been observed in LHCD discharges. The magnitude of the rotation is core localized and increases with LHCD power, decreases with electron density and decreases with the  $n_{||}$  of the launched waves. The negative core radial electric field is consistent with an inward shift of fast electron orbits. The rotation evolves on a time scale similar to the current relaxation time but slow compared to the momentum

confinement time. The rotation is well correlated with changes in the internal inductance, and peaking of the core electron density, as well as ion and electron temperatures.

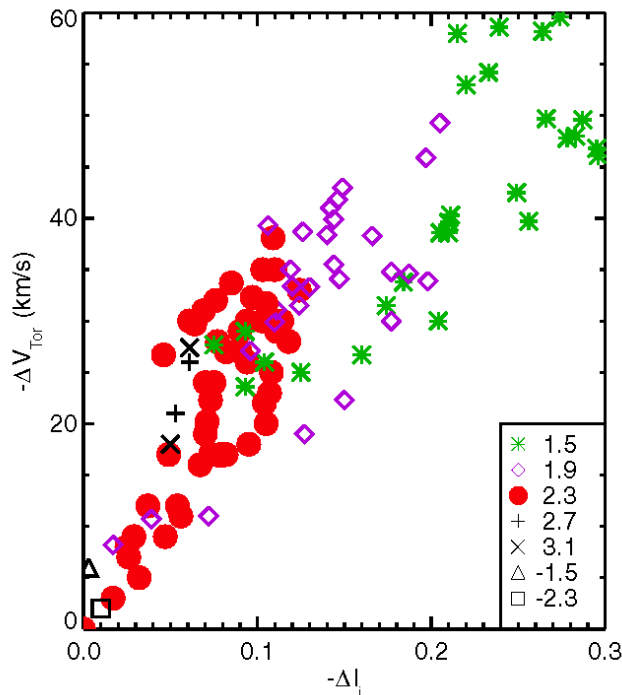


FIG.6. The change in the central rotation velocity as a function of the change in the internal inductance with LHCD. The points are sorted by  $n_{||}$ .

#### 5. Acknowledgements

The authors thank N. Fisch for enlightening discussions, J. Terry for  $D_\alpha$  measurements and the Alcator C-Mod operations, LHCD and ICRF groups for expert running of the tokamak. Work supported at MIT by DoE Contract No. DE-FC02-99ER54512.

## 6. References

- [1] N.J.Fisch, Rev. Mod. Phys. **59** (1987) 175.
- [2] M.Porkolab et al., Phys. Rev. Lett. **53** (1984) 450.
- [3] F.X.Soldner and JET Team, Plasma Phys. Contr. Fusion **39** (1997) B353.
- [4] S.Ide et al., Nucl. Fusion **40** (2000) 445.
- [5] P.T.Bonoli et al., Fusion Sci. Technol. **51** (2007) 401.
- [6] O.Sauter et al., Phys. Plasmas **6** (1999) 2834.
- [7] R.C.Wolf, Plasma Phys. Contr. Fusion **45** (2003) R1.
- [8] J.W.Connor et al., Nucl. Fusion **44** (2004) R1.
- [9] J.E.Rice et al., Nucl. Fusion **41** (2001) 277.
- [10] C.L.Fiore et al., Phys. Plasmas **8** (2001) 2023.
- [11] J.E.Rice et al., Nucl. Fusion **42** (2002) 510.
- [12] S.J.Wukitch et al., Phys. Plasmas **9** (2002) 2149.
- [13] J.E.Rice et al., Nucl. Fusion **43** (2003) 781.
- [14] C.L.Fiore et al., Fusion Sci. Technol. **51** (2007) 303.
- [15] X.Litaudon et al., Plasma Phys. Contr. Fusion **38** (1996) 1603.
- [16] Z.A.Pietrzyk et al., Phys. Rev. Lett. **86** (2001) 1530.
- [17] V.Pericoli Rindolfini al., Nucl. Fusion **43** (2003) 469.
- [18] E.J.Strait et al., Phys. Rev. Lett. **74** (1994) 2483.
- [19] L.-J.Zheng et al., Phys. Rev. Lett. **95** (2005) 255003.
- [20] J.E.Rice et al., Nucl. Fusion **47** (2007) 1618.
- [21] J.E.Rice et al., Fusion Sci. Technol. **51** (2007) 288.
- [22] E.S.Marmar et al., Fusion Sci. Technol. **51** (2007) 261.
- [23] A.Ince-Cushman et al., "Spatially Resolved High Resolution X-ray Spectroscopy for Magnetically Confined Fusion Plasmas", accepted for publication in Rev. Sci. Instrum. (2008).
- [24] N.P.Basse et al., Fusion Sci. Technol. **51** (2007) 476.
- [25] L.L.Lao et al., Nucl. Fusion **25** (1985) 1611.
- [26] A.Ince-Cushman et al., "Observations of Self Generated Flows in Tokamak Plasmas with Lower Hybrid Driven Current", submitted to Phys. Rev. Lett. (2008).
- [27] M.Greenwald et al., Fusion Sci. Technol. **51** (2007) 266.
- [28] W.D.Lee et al., Phys. Rev. Lett. **91** (2003) 205003.
- [29] J.E.Rice et al., Nucl. Fusion **44** (2004) 379.
- [30] A.Scarabosio et al., Plasma Phys. Contr. Fusion **48** (2006) 663.
- [31] B.P.Duval et al., Plasma Phys. Contr. Fusion **49** (2007) B195.
- [32] N.J.Fisch and C.F.F.Karney, Phys. Fluids **24** (1981) 27.